Ligand-Controlled Rates of Photoinduced Electron Transfer in Hybrid CdSe Nanocrystal/Poly(viologen) Films

Mario Tagliazucchi, Daniel B. Tice, Christina M. Sweeney, Adam J. Morris-Cohen, and Emily A. Weiss*

Department of Chemistry, Northwestern University, 2145 Sheridan Road, Evanston, Illinois 60208-3113, United States

ABSTRACT

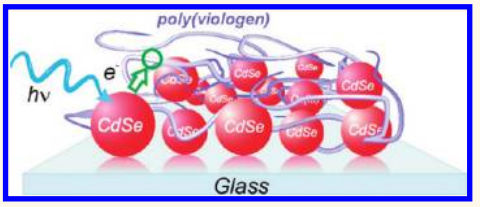

This paper describes a study of the rates of photoinduced electron transfer (PET) from CdSe quantum dots (QDs) to poly(viologen) within thin films, as a function of the length of the ligands passivating the QDs. Ultrafast (<10 ps), quantitative PET occurs from CdSe QDs coated with HS-$(CH_2)_n$-COOH for n = 1, 2, 5, and 7 to viologen units. The observed decrease in the magnitude of the PET rate constant with n is weaker than that expected from the decay of the electron tunneling probability across extended all-*trans* mercaptocarboxylic acids but well-described by electron tunneling across a collapsed ligand shell. The PET rate constants for films with n = 10 and 15 are much slower than those expected based on the trend for n = 1–7; this deviation is ascribed to the formation of bundles of ligands on the surface of the QD that make the tunneling process prohibitively slow by limiting access of the viologen units to the surfaces of the QDs. This study highlights the importance of molecular-level morphology of donor and acceptor materials in determining the rate and yield of interfacial photoinduced electron transfer in thin films.

KEYWORDS: CdSe quantum dot · photoinduced electron transfer · intermolecular structure · poly(viologen) · layer-by-layer deposition · transient absorption

This paper describes a study of the rate of photoinduced electron transfer (PET) from colloidal CdSe quantum dots (QDs) to poly(viologen) (PV) within a thin film upon resonant photoexcitation of the QDs. Ultrafast transient absorption measurements reveal that the length of the ligands coordinated to the QD surfaces dictates the rate of the PET process. Films comprising PV and CdSe QDs coated with mercaptocarboxylic acids, HS-$(CH_2)_n$-COOH, with n = 1–7 have average PET time constants of less than 10 ps and quantitative yields of PET. In contrast, films comprising CdSe QDs coated with longer ligands (n = 10 and 15) exhibit photoexcited electron lifetimes that are comparable to those observed in the absence of PV. We[1] and others[2–5] have previously demonstrated that molecular viologens in solution can accept electrons from photoexcited CdSe and CdS QDs in the sub-10 ps time scale. These studies, and others quantifying the rates of PET from cadmium and lead chalcogenide QDs to redox-active species in solution (such as anthraquinone,[6] organometallic complexes,[7] and TiO_2 colloids[8–10]), point to the binding equilibrium,[1] the energetic alignment of the frontier orbitals of the QD and the charge acceptor,[7,10] the thickness of an inorganic shell,[2,6,11] and the length of the linker between the QD and the redox species[12] as key factors controlling the rate of PET. Mechanistic analysis of PET between QDs and redox partners embedded in a solid matrix has received less attention than the solution case, despite its clear importance in solar energy conversion,[13] photodetection,[14] and light-emitting[15] technologies. The present work is the first to report PET between QDs and a solid-state polymeric viologen.

The variables affecting photoinduced charge separation in solution and films are not necessarily the same: in a film, the dynamic binding equilibrium between donor and acceptor is irrelevant, but the area of the donor/acceptor interface, which is determined by the deposition technique and phase segregation,[16,17] is critical. While small-molecule redox partners in solution-phase systems can penetrate the ligand shell of the QD to achieve a PET-active configuration,[2,3] this penetration may not be possible in dry films, especially with a conformationally constrained polymeric redox partner such as the poly(viologen) studied here. In the solid-state case, therefore, the length of the ligands capping the QD, and their intermolecular structure

* Address correspondence to e-weiss@northwestern.edu.

Received for review September 26, 2011 and accepted November 8, 2011.

Published online November 08, 2011
10.1021/nn203683s

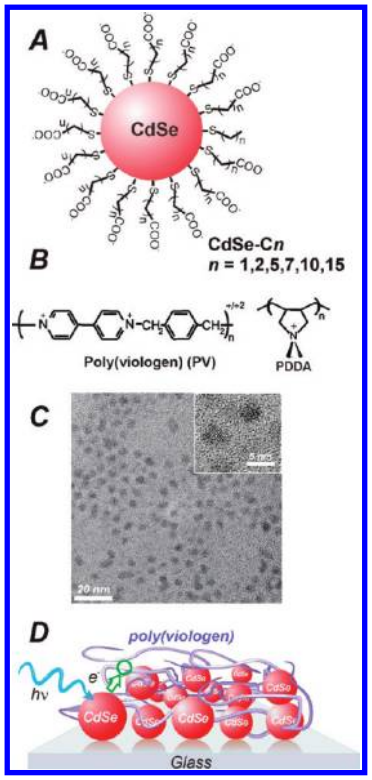

Figure 1. (A) Structure of the mercaptocarboxylic-acid-coated QDs used in this work. (B) Structure of the polymers used in this work. (C) TEM image for CdSe-C10. (D) Scheme of multilayer films of CdSe QDs coated by mercaptocarboxylic acids and PV on glass substrates (the $(PSS/PDDA)_2$ adhesion block is not shown in the scheme). Photoinduced electron transfer from the CdSe to the PV (green arrow) occurs upon selective illumination of the QDs.

within the capping monolayer, dictates the size and shape of the barrier for electron tunneling and determines the PET rate.

In this work, we demonstrate the importance of the nanoscopic morphology of the redox partners in determining the PET rate between CdSe QDs and poly(viologen) in layer-by-layer self-assembled films. Layer-by-layer-deposited films of redox polymers and QDs of different materials have been previously proposed as active layers in solar cells.[16,18] We systematically study the rate of PET with transient absorption spectroscopy as a function of the length of the ligands passivating the QDs and show that the PET time constants cannot be predicted by a model that describes electron tunneling through all-*trans*-extended ligand molecules, the type of model that is appropriate in the case of a conformationally rigid organic shell[19] or an inorganic shell.[2,6,11] We derive instead a simple quantitative model of PET that is based on the description of the ligand shell as a fluid and compact layer. On the basis of the results obtained by thorough characterization of the films using complementary techniques (tapping-mode AFM, XPS, ATR-FTIR, and UV−vis spectroscopy), we discuss how this molecular organization impacts the electron-transfer kinetics across the QD/PV interface.

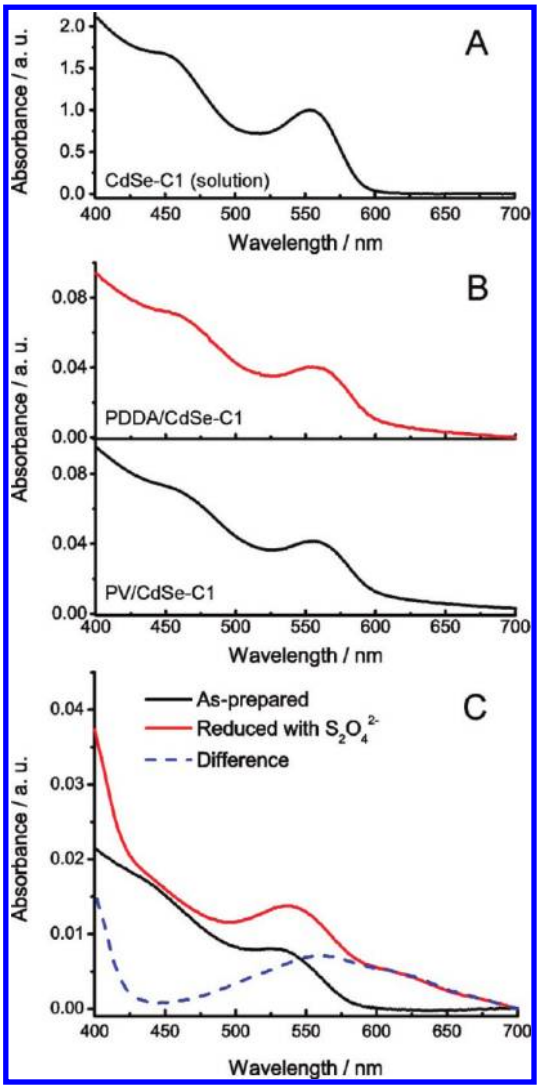

Figure 2. (A) Absorption spectra of the CdSe-C1 QDs in aqueous solution. (B) Absorption spectra of $(PDDA/PSS)_2$-$(PV/CdSe-C1)_4PV$, and $(PDDA/PSS)_2(PDDA/CdSe-C1)_3PDDA$ films on glass slides (only one side of the substrate is covered by the film). (C) Spectra for $(PDDA/PSS)_2(PV/CdSe-C1)_4PV$ film immersed in water (black line) and after reduction with a 10 mM $Na_2S_2O_4$ aqueous solution inside an airtight cell purged with nitrogen (red line). The blue dashed line is the difference between the spectra (the feature at 560 nm corresponds to $V^{1+\bullet}$).

RESULTS AND DISCUSSION

Synthesis and Characterization of the CdSe QDs and PV Redox Centers and the Layer-by-Layer Films. Figure 1A,B shows diagrams of the QD and poly(viologen) (PV) building blocks of the multilayer assemblies. We prepared water-soluble CdSe QDs by exchanging the alkylphosphonate[20] native ligands of organic-soluble CdSe QDs synthesized *via* an organometallic route with mercaptocarboxylic acids, $HS-(CH_2)_n-COOH$, of a series of lengths, n = 1, 2, 5, 7, 10, and 15 (all samples of water-soluble QDs were prepared from the same synthetic batch of organic-soluble QDs). The Experimental Methods section gives details of

TABLE 1. Position of the First Excitonic Peak, Cd:S and Cd:Se Atomic Ratios and Calculated Ligand Surface Coverages for CdSe-C*n* QDs in Solution[a]

sample	position of the excitonic peak	Cd:Se (EDS[b])	Cd:S (EDS[b])	Cd:Se (XPS[c])	Cd:S (XPS[c])	ligand surface coverage/chains · nm^{-2} [d]
CdSe in hexanes	549.7	1.8 ± 0.2	na	nd	na	na
CdSe-C1	553.3	1.8 ± 0.1	1.6 ± 0.1	1.63	1.86	5.6 ± 0.4
CdSe-C2	550.7	1.5 ± 0.1	2.3 ± 0.4	nd	nd	3.9 ± 0.7
CdSe-C5	549.1	1.1 ± 0.4	2.1 ± 0.9	nd	nd	4.3 ± 1.9
CdSe-C7	549.0	1.2 ± 0.1	2.0 ± 0.3	1.52	1.82	4.4 ± 0.6
CdSe-C10	554.4	1.9 ± 0.2	1.3 ± 0.2	nd	nd	6.7 ± 0.8
CdSe-C15	551.1	1.7 ± 0.4	1.5 ± 0.3	1.81	1.36	5.8 ± 1.1

[a] na, not applicable; nd, not determined. [b] Determined from TEM/EDS measurements on CdSe-C*n* QDs. [c] Determined from XPS measurements on PV/CdSe-C*n* films. [d] Calculated from EDS Cd:S ratio, assuming spherical shape and r_{core} = 1.5 nm; see Supporting Information.

the QD synthesis and ligand exchange. Hereafter, we will refer to the water-soluble QDs as CdSe-C*n*, where *n* is the number of methylene spacer groups in the mercaptocarboxylic acid ligand. Figures 1C and 2A show a representative transmission electron micrograph (TEM) image and an absorption spectrum of the CdSe-C*n* QDs, respectively. Table 1 lists the positions of the first excitonic peak for CdSe-C*n*, *n* = 1−15 (Figure S1 in the Supporting Information shows the absorption spectra for these samples) and the elemental composition measured by energy-dispersive spectroscopy (EDS) within the TEM. We observed no systematic trend between *n* and the Cd:Se ratio, the Cd:S ratio, or the first excitonic peak position; we therefore ascribe the sample-to-sample variation of these quantities to synthetic variability and/or experimental error in the characterization, rather than to an effect of the length of the ligands. We synthesized poly(*p*-xylyl viologen) (PV) following a previously published synthesis[21] and characterized it with ^{1}H NMR, UV−vis spectroscopy, and spectroelectrochemistry (see Supporting Information).

We prepared QD/PV films (Figure 1D) by layer-by-layer (LbL) self-assembly[22−24] on clean glass substrates that we modified with a $(PDDA/PSS)_2$ adhesion layer. The thickness of a representative film, $(PDDA/PSS)_2(PV/CdSe\text{-}C2)_6PV$ on glass, measured by AFM, was 56 ± 10 nm. In addition to PV/CdSe-C*n* films, we prepared films using the non-redox-active polycation poly(diallyldimethylammonium) (PDDA) in place of the PV as control samples where PET is not feasible. The LbL method produces homogeneous large-area films with high optical quality (see Figure S2 in the Supporting Information) that are well-suited for spectroscopic studies and allows fine intermixing of the components,[16] which is desirable for efficient PET. Films prepared in this study comprise between three and six PV/CdSe-C*n* or PDDA/CdSe-C*n* bilayers. For a given system, we did not observe any correlation between thickness and the normalized kinetic traces from the transient absorption experiments.

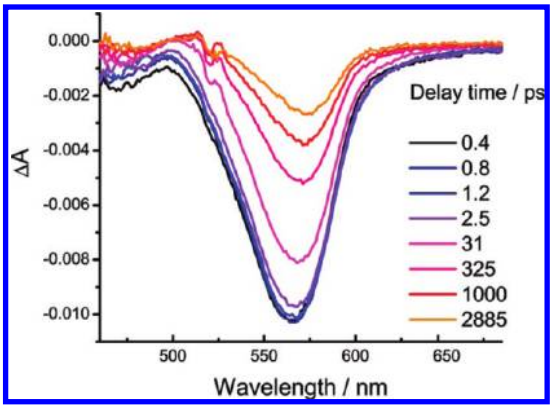

Figure 3. Transient absorption spectra for a $(PDDA/PSS)_2$-$(PDDA/CdSe\text{-}C1)_3PDDA$ film at different pump−probe delay times. The negative feature is the ground-state bleach (B1) of the QDs; this feature recovers due to depopulation of the $1S_e$ state from electron trapping and electron−hole recombination.

Figure 2B shows representative ground-state absorption spectra for PV/CdSe-C*n* and PDDA/CdSe-C*n* LbL films. In both cases, the spectra of the films resemble that of the isolated QDs since neither of the polycations absorbs light in the visible range (Figure S3 in the Supporting Information shows the absorption spectrum of isolated PV). We also acquired ground-state absorption spectra of the PV/CdSe-C*n* films before and after chemical reduction with a 10 mM $Na_2S_2O_4$ solution under inert atmosphere (Figure 2C). The difference spectrum reveals a broad absorption band with a maximum at 560 nm and a shoulder at 610−620 nm; these features correspond to the reduced viologen species.[25,26] This band is also apparent in electrochemically reduced films (Figure S6 in the Supporting Information). We used XPS to analyze the composition of the films. The Cd:S and Cd:Se ratios for PV/CdSe-C*n* films are similar to those observed for the CdSe-C*n* nanoparticles by EDS/TEM (Table 1); thus neither ligand desorption nor etching occurs during the LbL deposition.

Electron Transfer Occurs from Photoexcited CdSe QDs to PV. Figures 3 and 4 show chirp-corrected transient absorption (TA) spectra at different delay times for

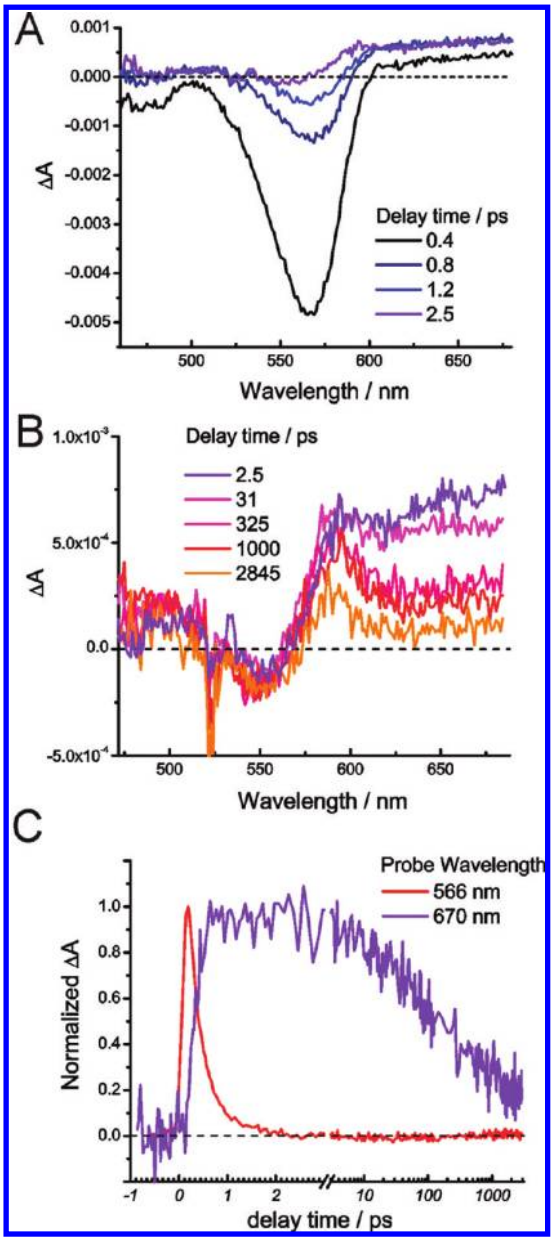

Figure 4. (A) Transient absorption spectra for a (PDDA/PSS)$_2$(PV/CdSe-C1)$_4$PV film for different pump−probe delay times between 0.4 and 2.5 ps. (B) Same plot as in A for pump−probe delay times between 2.5 and 2845 ps. (C) Kinetic traces at the peak of the B1 feature (566 nm, the trace was normalized and inverted) and at 670 nm (normalized trace) for the experiment in panels A and B.

the PDDA/CdSe-C1 and PV/CdSe-C1 films, respectively; the spectra of the PV/CdSe-C1 films are representative of those for $n = 1-7$. For delay times shorter than 0.5 ps, these spectra are dominated by the ground-state bleach (B1) feature at 565 nm, which results from saturation of the $1S_e-1S_{h3/2}$ interband optical transition.[27] In CdSe QDs, the amplitude of the B1 signal is directly correlated with the population of electrons in the conduction band ($1S_e$ level) but is insensitive to the hole population due to the near-degeneracy of the valence band states.[27−29] The B1 feature

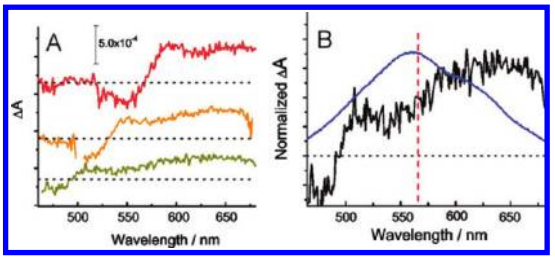

Figure 5. (A) Transient absorption spectra at a delay time of 20 ps for PV/CdSe films made of QDs of different sizes. From top to bottom, the position of the first excitonic peak is 554 (same as CdSe QDs as in Figures 3 and 4), 507, and 484 nm. The CdSe QDs in these experiments are coated with mercaptoacetic acid (n = 1). (B) Comparison between the spectra of the reduced viologen obtained by chemical reduction (blue line) and by photoinduced electron transfer within TA experiments (black line, bottom spectrum in A). The dashed vertical red line indicates the position of the bleach for the CdSe-Cn QDs with the first excitonic peak at 554 nm.

decays completely in ~1 ps for the PV/CdSe-C1 film, while in the absence of the PET decay pathway (PDDA/CdSe-C1 film), the bleach is present in the TA spectrum even for the longest delay time under study (3 ns).

The TA spectra for PV/CdSe-C1 at delay times longer than 0.4 ps also exhibit a broad, positive transient feature at longer wavelengths than the bleach. The dynamics for bleach recovery at 556 nm and formation of the feature at 670 nm (Figure 4C) are anticorrelated; this observation indicates that the 670 nm feature corresponds to the reduced viologen ($V^{1+\bullet}$) units in the polymer, and that the depopulation of the CdSe $1S_e$ occurs through electron transfer to PV. There is some convolution between the 670 nm feature and the transient features of the QD; therefore, in order to confirm this assignment, we acquired TA spectra for PV/CdSe films prepared with QDs of different sizes (first excitonic peaks at 484, 507, and 554 nm, Figure 5A). Transient features from the QD shift to higher energy as the size of the QD decreases, while the 670 nm feature remains at the same energy; this evidence supports the assignment of the 670 nm feature to $V^{1+\bullet}$. The assignment of the spectral features discussed above is further supported by a principal component analysis of the TA data (Figure S12 in the Supporting Information).

Figure 5B shows that the $V^{1+\bullet}$ feature in the TA experiments (as shown in the TA spectrum for the smallest QDs in Figure 5A) is shifted to lower energy with respect to that of chemically (Figure 2C) or electrochemically (Figure S6 in the Supporting Information) reduced PV, such that this band overlaps with the bleach of the CdSe-Cn QDs much less than what it is expected from the chemical reduction experiments. The bleach feature shown in Figure 5B therefore never becomes positive and shows no kinetics after 2.5 ps (as would occur if it were contaminated with signal from PV). A probable explanation for the origin of the hypsochromic shift of the reduced

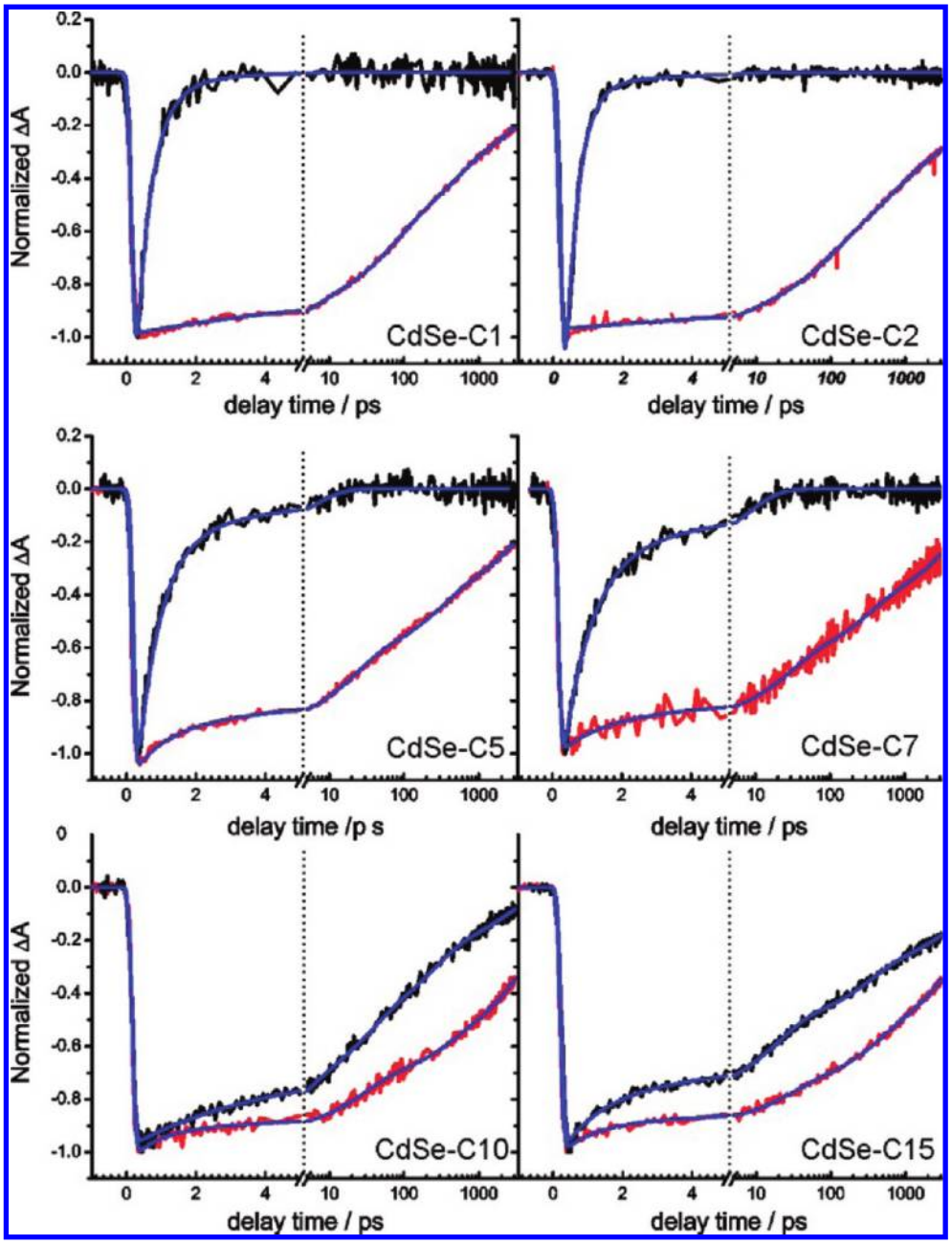

Figure 6. Representative normalized B1 traces for $(PDDA/PSS)_2(PV/CdSe\text{-}Cn)_mPV$ films (red trace) and for $(PDDA/PSS)_2(PV/CdSe\text{-}Cn)_mPDDA$ films (black curves, $m = 4-6$) with $n = 1-15$. Blue curves show the best fit with a sum of exponentials as described in the text.

viologen band in the TA spectrum relative to that of the chemically reduced PV is that the TA experiments are performed on dry films, while the chemical/electrochemical reduction is done in aqueous solutions. The molecular environments of PV in these two experiments are very different in terms of local dielectric constant, solvation, chain conformation, counterion distribution and mobility, and/or intramolecular interactions. For example, it has been reported that the spectrum of a double-bridged viologen radical cation embedded in polymer films has a maximum at 628 nm, which is lower energy than that observed in the same conditions for the monomeric benzylviologen radical cation (604 nm).[30] The authors explained the effect as a delocalization of the radical electron for the viologen dimer due to intramolecular π-interaction between rings; these interactions are also likely to occur in PV dry films but can be disrupted in solution due to solvation of the viologen units.

Dynamics of Photoinduced Electron Transfer. Figure 6 displays the kinetic traces at the peak of the ground-state bleach feature (B1) for a series of multilayer films, PV/CdSe-C*n*, with $n = 1, 2, 5, 7, 10$, and 15. For a given n, we measured at least three separately prepared PV/CdSe-C*n* films; the plots show representative traces. In the absence of PET, and in the low fluence regime

(where the expectation value of biexciton formation is negligible), the decay of the B1 signal occurs due to a combination of electron−hole radiative and nonradiative recombination and surface-mediated electron trapping.[31,32] In the case of the CdSe-C*n* QDs used in this study, radiative recombination is prevented by picosecond-to-subpicosecond trapping of the excitonic hole by the thiolate headgroups[33] (CdSe-C*n* QDs do not luminesce in solution or films); in the absence of a redox partner, the $1S_e$ level is therefore depleted by electron-trapping processes or nonradiative recombination with a trapped hole. We henceforth refer to the depopulation of the $1S_e$ level by these processes as "intrinsic electron decay".

We fit the B1 kinetic traces for PDDA/CdSe-C*n* (in the absence of the PV electron acceptor) with a sum of four exponential functions convoluted with the instrument response function (four is the minimum number of exponentials required to obtain randomly distributed residuals) (eq 1)

$$\Delta A(t) = \mathrm{IRF} \otimes \sum_{i=1}^{4} A_i \exp\left(-\frac{t}{\tau_i}\right) \qquad (1)$$

where A_i and τ_i are the amplitude and the time constant, respectively, associated with the *i*th exponential function. The best-fit parameters (summarized in Table 2 and Table S1 in the Supporting Information) indicate no systematic trends in the time constants for intrinsic electron decay for PDDA/CdSe-C*n* films with *n*. We also fit the B1 kinetic traces for PDDA/CdSe-C*n* with a sum of three stretched exponentials, but this fitting function yields less consistent results, involves more fitting parameters, and has a less clear physical interpretation than the sum of four exponentials (see Supporting Information).

Figure 6 shows that, for PV/CdSe-C*n* with *n* = 1−7, the B1 feature decays completely within 15 ps after photoexcitation due to electron transfer to the PV. The decay rate of the bleach is much faster for these films than for films of PDDA/CdSe-C*n*, in which electrons only undergo intrinsic decay; the separation of time scales between the rates of the PET process and the rates of intrinsic electron decay allows us to obtain the PET time constants by analyzing the B1 signal (Table 2 and Tables S2 and S3 in the Supporting Information). The dominance of the PET component in the B1 decay is evident when considering that, after 5 ps, ∼87% of the B1 signal is still present for PDDA/CdSe-C*n*, but only ∼6% is still present for the PV/CdSe-C*n* multilayers (these numbers are an average over all films with *n* = 1−7). We could, alternatively, quantify the PET rate by fitting the dynamics of the reduced viologen signal,[1] but this feature has low signal-to-noise in the PV/CdSe-C*n* spectra.

Figure 6 also shows that, for PV/CdSe-C10 and PV/CdSe-C15, the decay of the B1 feature is much slower than that for PV-CdSe-C*n* with *n* = 1−7, and the signal

TABLE 2. Best-Fit Parameters Obtained from the Analysis of the B1 Kinetic Traces in Figure 6 for PDDA/CdSe-C*n* and PV/CdSe-C*n* Films with a Sum of Two or Four Exponentials (eq 1)

PDDA/CdSe-C*n*

n	A_1	A_2	A_3	A_4	τ_1/ps	τ_2/ps	τ_3/ps	τ_4/ps
1	0.11	0.26	0.26	0.35	5.5	61.2	418	5755
2	0.08	0.22	0.26	0.41	9.1	86.1	551	8679
5	0.19	0.26	0.23	0.40	1.0	19.9	269	4354
7	0.14	0.22	0.22	0.43	1.3	25.4	288	5473
10	0.11	0.19	0.15	0.58	0.8	25.7	326	5808
15	0.12	0.14	0.19	0.56	1.0	25.6	359	6425

PV/CdSe-C*n*

n	A_1	A_2	A_3	A_4	τ_1/ps	τ_2/ps	τ_3/ps	τ_4/ps
1	1.26	0.17			0.42	1.3		
2	1.51	0.06			0.37	2.5		
5	1.02	0.22			0.63	2.2		
7	0.92	0.25			0.83	7.8		
10	0.21	0.25	0.28	0.24	3.3	27.5	222	2884
15	0.22	0.27	0.21	0.30	1.2	18.2	305	6072

from the $V^{1+\bullet}$ units in the polymer is barely discernible from the noise. In fact, for PV-CdSe-C*n* (*n* = 10 and 15), the dynamics of the B1 feature are very similar to those observed for PDDA/CdSe-C*n* with *n* = 10 and 15. We cannot, therefore, separate the contribution of PET from that of intrinsic electron decay in these films. In the following analysis, we will present a mechanism for the dependence of the PET rate on ligand length for *n* = 1−7 and propose an explanation for the slow PET rates observed for *n* = 10 and 15.

Collapsed Ligand Shell Model for the Effect of Ligand Length on the PET Rate (for *n* = 1−7). Two is the minimum number of exponentials required to fit the B1 decay traces for PV/CdSe-C*n* with *n* = 1−7. The two exponentials required to fit the B1 transients are probably an approximation to the real multiexponential behavior of the system rather than an indication of the presence of two well-defined decay pathways or QD−viologen subpopulations. The fact that a single exponential fails to fit these transients reflects a heterogeneous distribution of the PET rates. This heterogeneity can arise from (i) an inhomogeneous distribution of donor−acceptor geometries—that is, in the number of viologens within a given tunneling distance,[1] the viologen orientation, and the distance of the viologen to the CdSe surface; (ii) an inhomogeneous chemical environment (local dielectric constant and charge distribution); (iii) the presence of multiple PET pathways for a given viologen−CdSe configuration; (iv) the heterogeneity of the QD sample (surface chemistry, shape, and size); or (v) (most likely) a combination of all of these factors. Fitting the traces with a single stretched exponential yields a similar ligand length dependence of the time constants (see Figure S9 in the Supporting Information). We chose to use the sum of

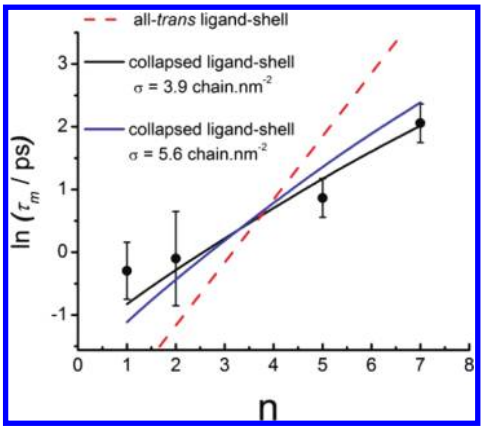

Figure 7. Plot of the logarithm of the intensity-averaged PET time constants for PV/CdSe-C*n* films as a function of *n*. For each *n*, the reported value and the error bar correspond to the average and the standard deviation of the ln(τ_m) for at least three separately prepared samples. The red dashed line shows the best-fit curve with eq 3 using *A* as the only fitting parameter ($A = 2.7 \times 10^{-3}$ ps), $\beta = 0.8$ Å^{-1}, and $d_{shell} = n \times 1.26$ Å + 3.4 Å (*i.e.*, electron tunneling across all-*trans* ligands). Solid lines show the predictions of eq 3 and the collapsed-shell model (eq 4) for the fixed parameters $\beta = 0.8$ Å^{-1}, $r_{core} = 1.5$ nm, and $\sigma = 3.9$ chains·nm^{-2} (black line) or $\sigma = 5.6$ chains·nm^{-2} (blue line) and using *A* as a fitting parameter, $A = 2.6 \times 10^{-2}$ ps (black line) or 7.0×10^{-3} ps (blue line).

exponentials as our fitting function in order to keep consistency with the multiexponential fitting function used for PDDA/CdSe-C*n* films and because fitting some decay traces with a stretched exponential yielded stretched coefficients larger than one, a result that lacks a straightforward physical interpretation (Table S4 in the Supporting Information).

In order to compare the characteristic PET time scales for different films, we calculated the intensity (second moment) average of the two best-fit time constants, τ_1 and τ_2, from the two-exponential fit function (eq 2). The plot of ln(τ_m) *versus n* in Figure 7 shows that this average time

$$\tau_m = \frac{\sum_{i=1}^{2} \tau_i^2 A_i}{\sum_{i=1}^{2} \tau_i A_i} \qquad (2)$$

constant for PET, τ_m, decreases with increasing *n* (for $n = 1-7$). Figure S8 in the Supporting Information shows that the time constants τ_1 and τ_2 both individually follow this trend. We first fit the plot in Figure 7 with the simple model for tunneling through a rectangular barrier (eq 3).[34] In eq 3, β is the tunneling decay constant, d_{shell} is the thickness of the ligand layer

$$\tau_{PET} = k_{PET}^{-1} = A\exp(\beta d_{shell}) \qquad (3)$$

that separates the viologen unit from the QD surface (the length of the tunneling barrier), and *A* is a pre-exponential factor that is assumed to be independent of the thickness of the tunneling barrier. Previous work on electron transfer through saturated all-*trans*-extended alkyl molecules[34−36] reports $\beta \sim 0.8$ Å^{-1} and $d_{shell} = d_{CH_2}n + d'$, where d_{CH_2} is the length of a CH_2 unit and d' is the *n*-independent length of the end groups (we determined $d_{CH_2} = 1.26$ Å and $d' = 3.4$ Å for the mercaptocarboxylic acids based on molecular models). The dashed line in Figure 7 shows that the literature value for β produces a much stronger dependence of τ_m on ligand length than we observe experimentally. A good fit to the experimental data, using $d_{CH_2} = 1.26$ Å and $d' = 3.4$ Å, rather requires a value of β of 0.3 Å^{-1}, which is abnormally low for electron tunneling through a saturated alkyl bridge.[34−36] We therefore suspect that the ligand shell of the QDs is not composed of *trans*-extended ligands.

In dry films, the ligands on the QD surface can form a compact film—that is, the ligand shell collapses—in order to maximize their packing efficiency. The low dielectric constant of the medium ensures that the carboxylate headgroups will be either paired with the polycation or a mobile cation or protonated. We expect, therefore, that, in the solid state, the electrostatic repulsion between charged headgroups will not hinder the collapse of the ligand shell. Equation 4 gives an expression (derived in the Supporting Information) for the thickness of a fully collapsed ligand layer on a spherical QD, based on simple geometric arguments. In eq 4, ρ_{ligand} and M_{ligand} are the *n*-dependent density and molecular weight of the ligands, σ is the ligand

$$d_{shell} = \left(\frac{3\sigma r_{core}^2 M_{ligand}}{\rho_{ligand} N_A} + r_{core}^3\right)^{1/3} - r_{core} \qquad (4)$$

surface coverage, r_{core} is the radius of the QD inorganic core, and N_A is Avogadro's number. This model accurately describes the weak dependence of the PET time constants on the ligand length observed for $n = 1-7$ (solid lines in Figure 7) using $\beta = 0.8$ Å^{-1} for a *trans*-extended monolayer and $\sigma = 3.9$ (black) or 5.6 (blue) chains·nm^{-2} (these values correspond to the surface coverage range measured for CdSe-C*n* with $n = 1-7$, Table 1).

An alternative mechanism that could explain the dependence of τ_m on *n* is the penetration of the ligand shell by PV. We believe, however, that the observed trend cannot be attributed solely to penetration of an all-*trans* ligand shell by PV since previous work shows that positively charged methylene blue (MB), which is less conformationally restricted than PV, adsorbs on the outer surface of mercaptocarboxylate self-assembled monolayers on Au rather than penetrating into the layer.[37−39] The penetration of PV into the QD ligand shell is thus unlikely.

Possible Mechanisms for the Slow PET Rates Observed for PV/CdSe-C*n* Films with *n* = 10−15. The PET time constants predicted from the collapsed-shell model (eqs 3 and 4) for PV/CdSe-C*n* with $n = 10$ and 15 are $\tau = 108$ and 370

ps, respectively (in this calculation, we used the surface coverages reported in Table 1 for $n = 10$ and 15 and the best-fit value of $A = 2.6 \times 10^{-2}$ ps obtained from the fit in Figure 7). In these two samples, however, we experimentally observe that the bleach recovery is incomplete even after 3 ns (Figure 6). We are confident that this discrepancy between predicted and observed dynamics is not due to sample-to-sample variations or measurement errors because (i) we prepared at least three PV/CdSe-C*n* films for each *n*, and in all samples with $n \leq 7$, the B1 signal completely decayed within ~2−15 ps, while in all samples with $n \geq 10$, the decay was always incomplete after 3 ns; and (ii) films with fast ($n = 1-7$) and slow ($n = 10$ and 15) B1 decay rates were prepared and measured on the same day under almost identical conditions. The slow PET rates for $n = 10$ and 15 are also not due to a stoichiometric deficiency of viologens in the film because CdSe:viologen unit molar ratios (calculated from chemical reduction experiments, as that shown in Figure 2C) are uncorrelated with *n* and vary between 1:3.6 and 1:6.7 (see Supporting Information). This result is supported by ATR-FTIR measurements (Figure S7 in the Supporting Information) that show no systematic trend between *n* and the intensity of the characteristic PV band[40] at 1640 cm^{-1}. The excitonic peak positions slightly depend on *n* due to synthetic variability ($\Delta\lambda = \pm 2.7$ nm; see Table 1), and therefore, there is a small sample-to-sample variability in the energy of the LUMO levels and in the driving force of PET.[10] In the Supporting Information, however, we show that these differences cannot account for the inefficient PET observed for $n = 10$ and 15.

A plausible hypothesis for the fundamentally different behaviors of the films with $n = 1-7$ and $n = 10$ and 15 is that these longer alkyl chains form *trans*-extended rather than collapsed monolayers. Self-assembled monolayers on planar gold,[41,42] Au nanoparticles (NPs),[43] and SiO_2 NPs[44] show transitions from liquid-like disordered films to well-ordered compact monolayers as the ligand length increases. Interestingly, these transitions occur in a ligand length range (C5−C11,[41] C6−C10,[42] C5−C6[43]) similar to that where we observe the transition from fast to slow PET (between C7 and C10). The formation of compact SAMs obtained on planar substrates is frustrated for highly curved surfaces, where long ligands maximize their intermolecular hydrophobic interactions by forming bundles[45−49] (this mechanism is schematized in Figure 8). Assuming that the length of the bundles is equal to that of a *trans*-extended ligand, eq 3 predicts PET time constants of $\tau = 9.2$ ns (for $n = 10$) and 1.4 μs (for $n = 15$), with $A = 2.6 \times 10^{-2}$ ps (obtained from the fit in Figure 7), $\beta = 0.8$ Å^{-1}, and $d_{shell} = n \times 1.26$ Å + 3.4 Å. Both of these predicted time constants are larger than the time constants for the intrinsic electron decay, so the "bundling" mechanism could be responsible for the very low yield (or absence) of PET observed for PV/CdSe-C*n* with $n = 10$ and 15.

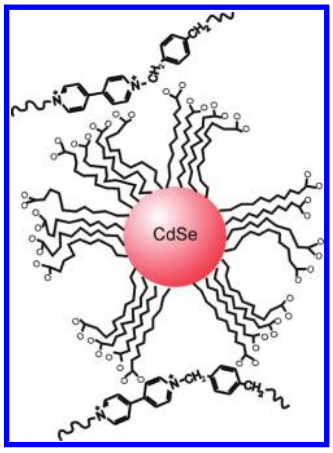

Figure 8. Scheme showing the increase in the tunneling distance due to the packing of ligands into all-*trans* bundles; this mechanism is proposed in the text to explain the unexpectedly slow PET kinetics observed for CdSe-C10 and CdSe-C15.

An additional factor that could contribute to the slow PET rates measured for PV/CdSe-C*n* films with $n = 10$ and 15 is the aggregation of QDs. Formation of QD aggregates would prevent the poly(viologen) from accessing QDs that are not at the surface of the aggregates and thereby prevent the redox centers from achieving a PET-active configuration. This mechanism is possible but unlikely for reasons that we detail in the Supporting Information.

CONCLUSIONS

We have demonstrated that photoinduced electron transfer (PET) occurs from CdSe QDs passivated by HS-$(CH_2)_n$-COOH ligands ($n = 1-7$) to poly(viologen) on the ultrafast time scale within a thin film. The distance dependence of the PET rate for these films indicates that the ligands assume a predominantly collapsed, rather than *trans*-extended, conformation. We have also shown, for the first time, a dramatic decrease of the PET rate upon increasing the length of the ligands on the QDs from $n = 7$ to $n = 10$ that cannot be accounted for with the length dependence exhibited by the shorter ligands. We propose that the unexpectedly slow PET for the systems with $n \geq 10$ is due to the association of the mercaptocarboxylic acid ligands into *trans*-extended bundles that increase the average tunneling distance for PET. Conclusively determining the contribution of this mechanism to the observed PET rate is difficult, but the important message is that the ligand shell on the QD plays a key role in controlling film morphology at the nanoscale, and that this morphology strongly impacts the rate of photoinduced charge separation. These considerations are uniquely important in solid-state PET.

Poly(viologen) shares some key advantages with molecular viologens (commonly used as solution-phase oxidizing agents) for the study of PET in QD systems. These advantages are (i) the ability to extract

electrons from CdSe on the picosecond time scale, (ii) the characteristic absorption band of the reduced species in the visible region, and (iii) the possibility to easily synthesize poly(viologen)s with different molecular architectures[25] (differing, for example, in their redox potentials[50]). A major finding of the present work is that, despite the rather low ratio of viologen units to CdSe QDs (3.6−6.7:1) in the QD/PV films, very efficient and quantitative PET occurs from the QDs to PV in cases where PET-active donor−acceptor configurations are possible. We partially attribute this efficiency to the LbL deposition method, which provides good intermixing between the NPs and the polymer due to electrostatic pairing between the carboxylate end groups of the thiols and the positively charged viologen groups. These results motivate studies of the effect of the passivating ligands on photoinduced charge separation rates in other QD/redox molecule systems, both in films and solution, and suggest that the conformational behavior of the "soft" components in hybrid QD/organic films must be considered in the design of devices based on these composite materials. Future work will focus at determining whether the ultrafast PET demonstrated in this report can be effectively used in a photocurrent generation or photocatalysis scheme.

EXPERIMENTAL METHODS

Materials. All reagents were used as received from Sigma-Aldrich, with the exception of cadmium stearate, which was used as received from MP Biomedicals, Inc.

Synthesis of Poly(*p*-xylyl viologen). Poly(*p*-xylyl viologen) was prepared according a previous published procedure.[21] Briefly, we reacted 6.4 mmol of 4,4′-bipyridine (1.0 g) and 6.4 mmol of *p*-dibromoxylene (1.69 g) in 68 mL of dry acetonitrile for 2 days at room temperature, and the as-obtained precipitate was filtered and vacuum-dried. The product was dissolved in water and purified by dialysis against water using a membrane with a 6000 MW cutoff for 7 days. The Supporting Information describes characterization of the final product.

Synthesis of CdSe Quantum Dots. We prepared the CdSe-C*n* QDs from a single batch of CdSe nanocrystals in hexanes (band-edge absorption at 550 nm) using the method described by Lilly *et al.*[51] A 12 mL aliquot of Cd/Se stock solution, made of 224 mmol trioctylphosphine (TOP), 49.8 mmol Cd stearate, and 46.8 mmol Se, was injected into a mixture of hexadecylamine (HDA, 8.03 mmol) and trioctylphosphine oxide 90% (TOPO, 5.02 mmol) at 320 °C under positive N_2 pressure with stirring. The formation of CdSe (red solution) immediately followed the injection; the reaction was allowed to proceed at 290 °C for 5 min and then quenched to a temperature <70 °C by fast addition of hexanes. This procedure yielded ∼1.4 μmol of CdSe QDs (after purification). We prepared the CdSe QDs of different sizes for the experiments in Figure 5 according to the procedure of Qu *et al.*,[52] with slight modifications.[20] A mixture of 90% TOPO (5.02 mmol), HDA (8.04 mmol), and Cd stearate (0.165 mmol) was dried for 1.5 h by heating at 105 °C in a three-neck round-bottom flask under positive nitrogen flow and stirring. The reaction flask was then heated to 320 °C, and 1 mL of a 1 M TOPSe solution in TOP (prepared and stored in a glovebox) was quickly added through a septum. We allowed the reaction to proceed at 290 °C until the desired QD size was achieved and then quickly quenched the reaction with hexanes.

Purification of CdSe Quantum Dots. The CdSe quantum dots remained in the reaction crude for 2 h to allow the precipitation of some free ligands, which we then separated from the QDs by centrifugation for 10 min at 3500 rpm. We decanted the supernatant (which contained the QDs) and precipitated them by addition of methanol, centrifuged the solution, and discarded the resulting clear supernatant. We then redispersed the QD containing pellet in hexanes, centrifuged the solution, and discarded the ligand-containing white pellet. The supernatant was then purified by precipitation with methanol, centrifugation, and redispersion in hexanes two additional times. The size and concentration of the purified CdSe QDs were determined from their UV−vis spectrum using literature calibrations curves.[53]

Ligand Exchange with Mercaptocarboxylic Acids. In order to prepare PV/CdSe *via* layer-by-layer self-assembly, we rendered QDs water-soluble by ligand exchange with mercaptocarboxylic acids of different lengths. We followed the procedure of Aldana *et al.*[54] with minor modifications. We introduced nitrogen-dried CdSe QDs (100 nmol) and a solution of the mercaptocarboxylic acid (1 mmol) in absolute ethanol into a three-neck round-bottom flask and adjusted the suspension to pH >10 with benzyltrimethylammonium hydroxide. The mixture was stirred for 24 h under nitrogen. The resulting suspension was centrifuged, and the pellet was dissolved in ∼10 mL of diluted NaOH solution (pH 10) to yield a clear solution. We precipitated the CdSe QDs by adding ∼20 mL of a 1:1 mixture of methanol/acetone and then centrifuged and redisolved the QDs in a NaOH solution of pH ∼10. We repeated the precipitation/redisolution procedure three times. The elemental analysis of CdSe-C*n* QDs (measured by energy-dispersive spectroscopy, EDS; see Supporting Information) reveals the presence of Cd, Se, and S, but not of P. This result indicates complete exchange of the native ligands (mainly *n*-octylphosphonate, OPA, and *P*′-*P*′-(di-*n*-octyl-)pyrophosphonate, PPA[20]) by the mercaptocarboxylic acids. The solutions used for LbL assembly had a pH of 7.5 ± 0.3 and a concentration of 1.0−2.0 μM of CdSe + 0.25 M NaCl.

Layer-by-Layer (LbL) Adsorption. We used either plasma-cleaned glass or ITO on glass (Delta Technologies) slides as substrates for the LbL assembly. A $(PDDA/PSS)_2$ adhesion layer was grown on these substrates by two cycles of immersing the substrate in a 10 mM PDDA + 0.5 M NaCl solution for 15 min, thoroughly rinsing the substrate with water, and then immersing the substrate in a 10 mM PSS + 0.5 M NaCl solution for 15 min and thoroughly rinsing the substrate with water (this adhesion layer was not used for samples prepared for XPS measurements in order to avoid the contribution of PSS to the S signal). We have used NaCl in the assembly solution to increase the thickness per bilayer, based on literature reports[55] and preliminary experiments on the CdSe/PDDA system. We built either a PV/CdSe-C*n* or a PDDA/CdSe-C*n* multilayer on top of the adhesion layer by sequential absorption of CdSe-C*n* and the respective polycation until the desired number of layers was obtained. In each adsorption step, the sample was immersed in the polycation or CdSe-C*n* solution for 15 min, thoroughly rinsed with water and dried with nitrogen. Films were terminated with the polycation in order to avoid having CdSe QDs within different environments (*i.e.*, nanoparticles inside the film and on the outer surface). Progressive photoetching of the CdSe QDs occurred for samples in contact with the electrolyte solution (but not for dried films) and manipulated under ambient light conditions; therefore, the LbL procedure was performed in the dark. After the LbL procedure was complete, the film was removed from one side of the substrate using a tissue paper soaked in methanol.

Transient Absorption Experiments. We conducted femtosecond transient absorption experiments using a tunable excitation pulse from an optical parametric amplifier, OPA (TOPAS-C, Light Conversion), pumped by the 1kHz, 100 fs, 795 nm output of a mode-locked regeneratively amplified Ti:sapphire laser (Solstice, Spectra Physics). The output from the OPA was

chopped to 500 Hz in a commercial TA spectrometer (Helios, Ultrafast Systems) to enable active background subtraction and obtain differential absorption spectra. The probe beam, a white-light continuum generated by focusing part of the 795 nm output of the laser through a sapphire plate, and the pump beam entered the sample through the clean side of the glass substrate and then overlapped on the coated side of the substrate with an IRF of 200 fs. The probe pulse was then collimated and focused into a fiber optic connected to a CCD array. The sizes of the pump and probe pulses at the position of the film were 730 ± 100 and 220 ± 50 μm, respectively. The pump laser was tuned 30 nm higher in energy than the absorption peak of the band-edge exciton in order to facilitate the subtraction of the scattered pump light. All measurements were performed at a fixed pump energy of 1.8 μJ/pulse, which corresponds to an expectation value for the excited state, $\langle N \rangle$, of ~0.2 and conducted in a nitrogen purged gas-flow chamber[56] in order to minimize possible photobrightening effects[56] as well as the reaction between oxygen and reduced viologen species. Two successive measurements of the same sample under the same conditions produced overlapping TA traces; this result indicates no long-term photodegration of the films.

Acknowledgment. This material is based upon work supported as part of the NERC (Non-Equilibrium Research Center), an Energy Frontier Research Center funded by the U.S. Department of Energy, Office of Science, Office of Basic Energy Sciences under Award Number DE-SC0000989. This work used instruments located in the NUANCE Center facilities, which are supported by the NSF-MRSEC, NSF-NSEC, and the Keck Foundation.

Supporting Information Available: Experimental details, ground-state absorption spectra of CdSe-C*n* QDs in film and solution, characterization of PV by UV−vis, ^{1}H NMR and spectroelectrochemistry, FTIR-ATR spectra of PV/CdSe-C*n* films, best-fit parameters for fits of the TA dynamics with sum of exponentials and stretched exponential functions, estimation of effect of the LUMO level of CdSe-C*n* on the PET time constants, derivation of eq 4, and AFM micrographs of PV/CdSe-C*n* films. This material is available free of charge *via* the Internet at http://pubs.acs.org.

REFERENCES AND NOTES

1. Morris-Cohen, A. J.; Frederick, M. T.; Cass, L. C.; Weiss, E. A. Simultaneous Determination of the Adsorption Constant and the Photoinduced Electron Transfer Rate for a CdS Quantum Dot−Viologen Complex. *J. Am. Chem. Soc.* **2011**, *133*, 10146–10154.
2. Dworak, L.; Matylitsky, V. V.; Breus, V. V.; Braun, M.; Basche, T.; Wachtveitl, J. Ultrafast Charge Separation at the CdSe/CdS Core/Shell Quantum Dot/Methylviologen Interface: Implications for Nanocrystal Solar Cells. *J. Phys. Chem. C* **2011**, *115*, 3949–3955.
3. Matylitsky, V. V.; Dworak, L.; Breus, V. V.; Basche, T.; Wachtveitl, J. Ultrafast Charge Separation in Multiexcited CdSe Quantum Dots Mediated by Adsorbed Electron Acceptors. *J. Am. Chem. Soc.* **2009**, *131*, 2424.
4. Jiang, Z. J.; Kelley, D. F. Hot and Relaxed Electron Transfer from the CdSe Core and Core/Shell Nanorods. *J. Phys. Chem. C* **2011**, *115*, 4594–4602.
5. Harris, C.; Kamat, P. V. Photocatalysis with CdSe Nanoparticles in Confined Media: Mapping Charge Transfer Events in the Subpicosecond to Second Timescales. *ACS Nano* **2009**, *3*, 682–690.
6. Zhu, H.; Song, N.; Lian, T. Wave Function Engineering for Ultrafast Charge Separation and Slow Charge Recombination in Type II Core/Shell Quantum Dots. *J. Am. Chem. Soc.* **2011**, *133*, 8762–8771.
7. Huang, J.; Stockwell, D.; Huang, Z. Q.; Mohler, D. L.; Lian, T. Q. Photoinduced Ultrafast Electron Transfer from CdSe Quantum Dots to Re-Bipyridyl Complexes. *J. Am. Chem. Soc.* **2008**, *130*, 5632.
8. Robel, I.; Subramanian, V.; Kuno, M.; Kamat, P. V. Quantum Dot Solar Cells. Harvesting Light Energy with CdSe Nanocrystals Molecularly Linked to Mesoscopic TiO_2 Films. *J. Am. Chem. Soc.* **2006**, *128*, 2385–2393.
9. Dibbell, R. S.; Youker, D. G.; Watson, D. F. Excited-State Electron Transfer from CdS Quantum Dots to TiO_2 Nanoparticles *via* Molecular Linkers with Phenylene Bridges. *J. Phys. Chem. C* **2009**, *113*, 18643–18651.
10. Robel, I.; Kuno, M.; Kamat, P. V. Size-Dependent Electron Injection from Excited CdSe Quantum Dots into TiO_2 Nanoparticles. *J. Am. Chem. Soc.* **2007**, *129*, 4136–4137.
11. Zhu, H. M.; Song, N. H.; Lian, T. Q. Controlling Charge Separation and Recombination Rates in CdSe/ZnS Type I Core−Shell Quantum Dots by Shell Thicknesses. *J. Am. Chem. Soc.* **2010**, *132*, 15038–15045.
12. Dibbell, R. S.; Watson, D. F. Distance-Dependent Electron Transfer in Tethered Assemblies of CdS Quantum Dots and TiO_2 Nanoparticles. *J. Phys. Chem. C* **2009**, *113*, 3139–3149.
13. Zhou, Y.; Eck, M.; Krüger, M. Bulk-Heterojunction Hybrid Solar Cells Based on Colloidal Nanocrystals and Conjugated Polymers. *Energy Environ. Sci.* **2010**, *3*, 1851–1864.
14. Szendrei, K.; Cordella, F.; Kovalenko, M. V.; Boeberl, M.; Hesser, G.; Yorema, M.; Jarzab, D.; Mikhnenko, O. V.; Gocalinska, A.; Saba, M.; *et al.* Solution-Processable Near-IR Photodetectors Based on Electron Transfer from PbS Nanocrystals to Fullerene Derivatives. *Adv. Mater.* **2009**, *21*, 683.
15. Bae, W. K.; Kwak, J.; Lim, J.; Lee, D.; Nam, M. K.; Char, K.; Lee, C.; Lee, S. Multicolored Light-Emitting Diodes Based on All-Quantum-Dot Multilayer Films Using Layer-by-Layer Assembly Method. *Nano Lett.* **2010**, *10*, 2368–2373.
16. McClure, S. A.; Worfolk, B. J.; Rider, D. A.; Tucker, R. T.; Fordyce, J. A. M.; Fleischauer, M. D.; Harris, K. D.; Brett, M. J.; Buriak, J. M. Electrostatic Layer-by-Layer Assembly of CdSe Nanorod/Polymer Nanocomposite Thin Films. *ACS Appl. Mater. Interfaces* **2010**, *2*, 219–229.
17. Ren, S.; Chang, L.-Y.; Lim, S.-K.; Zhao, J.; Smith, M.; Zhao, N.; Bulović, V.; Bawendi, M.; Gradečak, S. Inorganic−Organic Hybrid Solar Cell: Bridging Quantum Dots to Conjugated Polymer Nanowires. *Nano Lett.* **2011**, *11*, 3998–4002.
18. Kniprath, R.; Rabe, J. P.; McLeskey, J. T., Jr.; Wang, D.; Kirstein, S. Hybrid Photovoltaic Cells with II−VI Quantum Dot Sensitizers Fabricated by Layer-by-Layer Deposition of Water-Soluble Components. *Thin Solid Films* **2009**, *518*, 295–298.
19. Bakkers, E.; Roest, A. L.; Marsman, A. W.; Jenneskens, L. W.; de Jong-van Steensel, L. I.; Kelly, J. J.; Vanmaekelbergh, D. Characterization of Photoinduced Electron Tunneling in Gold/SAM/Q-CdSe Systems by Time-Resolved Photoelectrochemistry. *J. Phys. Chem. B* **2000**, *104*, 7266–7272.
20. Morris-Cohen, A. J.; Donakowski, M. D.; Knowles, K. E.; Weiss, E. A. The Effect of a Common Purification Procedure on the Chemical Composition of the Surfaces of CdSe Quantum Dots Synthesized with Trioctylphosphine Oxide. *J. Phys. Chem. C* **2010**, *114*, 897–906.
21. Factor, A.; Heinsohn, G. E. Polyviologens. A Novel Class of Cationic Polyelectrolyte Redox Polymers. *J. Polym. Sci., Part B* **1971**, *9*, 289–295.
22. Decher, G. Fuzzy Nanoassemblies: Toward Layered Polymeric Multicomposites. *Science* **1997**, *277*, 1232–1237.
23. Mamedov, A. A.; Belov, A.; Giersig, M.; Mamedova, N. N.; Kotov, N. A. Nanorainbows: Graded Semiconductor Films from Quantum Dots. *J. Am. Chem. Soc.* **2001**, *123*, 7738–7739.
24. Rogach, A. L.; Klar, T. A.; Lupton, J. M.; Meijerink, A.; Feldmann, J. Energy Transfer with Semiconductor Nanocrystals. *J. Mater. Chem.* **2009**, *19*, 1208–1221.
25. Sassoon, R. E.; Gershuni, S.; Rabani, J. Charge Separation in Photointiated Electron-Transfer Systems with Polyviologen Poly-electrolytes as Quenchers. *J. Phys. Chem.* **1985**, *89*, 1937–1945.
26. DeLongchamp, D. M.; Kastantin, M.; Hammond, P. T. High-Contrast Electrochromism from Layer-by-Layer Polymer Films. *Chem. Mater.* **2003**, *15*, 1575–1586.
27. Klimov, V. I.; Schwarz, C. J.; McBranch, D. W.; Leatherdale, C. A.; Bawendi, M. G. Ultrafast Dynamics of Inter- and Intraband Transitions in Semiconductor Nanocrystals:

Implications for Quantum-Dot Lasers. *Phys. Rev. B* **1999**, *60*, R2177–R2180.
28. Sewall, S. L.; Cooney, R. R.; Anderson, K. E. H.; Dias, E. A.; Kambhampati, P. State-to-State Exciton Dynamics in Semiconductor Quantum Dots. *Phys. Rev. B* **2006**, *74*, 235328.
29. Huang, J.; Huang, Z.; Jin, S.; Lian, T. Exciton Dissociation in CdSe Quantum Dots by Hole Transfer to Phenothiazine. *J. Phys. Chem. C* **2008**, *112*, 19734–19738.
30. Sun, X. H.; Yang, Y. K. Photochromism of Double-Bridged Viologens in a Polar Polymer Matrix. *J. Chem. Soc., Perkin Trans. 2* **1996**, 225–228.
31. Knowles, K. E.; McArthur, E. A.; Weiss, E. A. A Multi-Time-scale Map of Radiative and Nonradiative Decay Pathways for Excitons in CdSe Quantum Dots. *ACS Nano* **2011**, *5*, 2026–2035.
32. Klimov, V. I. Optical Nonlinearities and Ultrafast Carrier Dynamics in Semiconductor Nanocrystals. *J. Phys. Chem. B* **2000**, *104*, 6112–6123.
33. Guyot-Sionnest, P.; Wehrenberg, B.; Yu, D. Intraband Relaxation in Cdse Nanocrystals and the Strong Influence of the Surface Ligands. *J. Chem. Phys.* **2005**, *123*, 074709.
34. Adams, D. M.; Brus, L.; Chidsey, C. E. D.; Creager, S.; Creutz, C.; Kagan, C. R.; Kamat, P. V.; Lieberman, M.; Lindsay, S.; Marcus, R. A.; *et al.* Charge Transfer on the Nanoscale: Current Status. *J. Phys. Chem. B* **2003**, *107*, 6668–6697.
35. Nijhuis, C. A.; Reus, W. F.; Barber, J. R.; Dickey, M. D.; Whitesides, G. M. Charge Transport and Rectification in Arrays of SAM-Based Tunneling Junctions. *Nano Lett.* **2010**, *10*, 3611–3619.
36. Smalley, J. F.; Finklea, H. O.; Chidsey, C. E. D.; Linford, M. R.; Creager, S. E.; Ferraris, J. P.; Chalfant, K.; Zawodzinsk, T.; Feldberg, S. W.; Newton, M. D. Heterogeneous Electron-Transfer Kinetics for Ruthenium and Ferrocene Redox Moieties through Alkanethiol Monolayers on Gold. *J. Am. Chem. Soc.* **2003**, *125*, 2004–2013.
37. Benitez, G.; Vericat, C.; Tanco, S.; Lenicov, F. R.; Castez, M. F.; Vela, A. E.; Salvarezza, R. C. Role of Surface Heterogeneity and Molecular Interactions in the Charge-Transfer Process through Self-Assembled Thiolate Monolayers on Au(111). *Langmuir* **2004**, *20*, 5030–5037.
38. Tognalli, N. G.; Fainstein, A.; Vericat, C.; Vela, M. E.; Salvarezza, R. C. Exploring Three-Dimensional Nanosystems with Raman Spectroscopy: Methylene Blue Adsorbed on Thiol and Sulfur Monolayers on Gold. *J. Phys. Chem. B* **2006**, *110*, 354–360.
39. Vericat, C.; Lenicov, F. R.; Tanco, S.; Andreasen, G.; Vela, M. E.; Salvarezza, R. C. Building Complex Two-Dimensional Structures: Methylene Blue on Self-Assembled Monolayer-Covered Au(111). *J. Phys. Chem. B* **2002**, *106*, 9114–9121.
40. Zacharia, N. S.; Modestino, M.; Hammond, P. T. Factors Influencing the Interdiffusion of Weak Polycations in Multilayers. *Macromolecules* **2007**, *40*, 9523–9528.
41. Porter, M. D.; Bright, T. B.; Allara, D. L.; Chidsey, C. E. D. Spontaneously Organized Molecular Assemblies 0.4. Structural Characterization of Normal-Alkyl Thiol Monolayers on Gold by Optical Ellipsometry, Infrared-Spectroscopy, and Electrochemistry. *J. Am. Chem. Soc.* **1987**, *109*, 3559–3568.
42. Grumelli, D.; Mendez De Leo, L. P.; Bonazzola, C.; Zamlynny, V.; Calvo, E. J.; Salvarezza, R. C. Methylene Blue Incorporation into Alkanethiol Sams on Au(111): Effect of Hydrocarbon Chain Ordering. *Langmuir* **2010**, *26*, 8226–8232.
43. Hostetler, M. J.; Stokes, J. J.; Murray, R. W. Infrared Spectroscopy of Three-Dimensional Self-Assembled Monolayers: *N*-Alkanethiolate Monolayers on Gold Cluster Compounds. *Langmuir* **1996**, *12*, 3604–3612.
44. Jones, R. L.; Pearsall, N. C.; Batteas, J. D. Disorder in Alkylsilane Monolayers Assembled on Surfaces with Nanoscopic Curvature. *J. Phys. Chem. C* **2009**, *113*, 4507–4514.
45. Donakowski, M. D.; Godbe, J. M.; Sknepnek, R.; Knowles, K. E.; de la Cruz, M. O.; Weiss, E. A. A Quantitative Description of the Binding Equilibria of para-Substituted Aniline Ligands and CdSe Quantum Dots. *J. Phys. Chem. C* **2010**, *114*, 22526–22534.
46. Guo, P.; Sknepnek, R.; de la Cruz, M. O. Electrostatic-Driven Ridge Formation on Nanoparticles Coated with Charged End-Group Ligands. *J. Phys. Chem. C* **2011**, *115*, 6484–6490.
47. Sandberg, D. J.; Carrillo, J.-M. Y.; Dobrynin, A. V. Molecular Dynamics Simulations of Polyelectrolyte Brushes: From Single Chains to Bundles of Chains. *Langmuir* **2007**, *23*, 12716–12728.
48. Lane, J. M. D.; Grest, G. S. Spontaneous Asymmetry of Coated Spherical Nanoparticles in Solution and at Liquid–Vapor Interfaces. *Phys. Rev. Lett.* **2010**, *104*, 235501.
49. Ghorai, P. K.; Glotzer, S. C. Molecular Dynamics Simulation Study of Self-Assembled Monolayers of Alkanethiol Surfactants on Spherical Gold Nanoparticles. *J. Phys. Chem. C* **2007**, *111*, 15857–15862.
50. Zotti, G.; Zecchin, S.; Vercelli, B.; Berlin, A.; Grimoldi, S.; Bertoncello, R.; Milanese, L. Self-Assembled Monolayers and Electrostatically Self-Assembled Multilayers of Polyalkylviologens on Sulfonate-Modified Gold and Indium-Tin-Oxide Electrodes. *J. Electroanal. Chem.* **2005**, *580*, 330–339.
51. Lilly, G. D.; Whalley, A. C.; Grunder, S.; Valente, C.; Frederick, M. T.; Stoddart, J. F.; Weiss, E. A. Switchable Photoconductivity of Quantum Dot Films Using Cross-Linking Ligands with Light-Sensitive Structures. *J. Mater. Chem.* **2011**, *21*, 11492–11497.
52. Qu, L.; Peng, X. Control of Photoluminescence Properties of CdSe Nanocrystals in Growth. *J. Am. Chem. Soc.* **2002**, *124*, 2049–2055.
53. Yu, W. W.; Qu, L.; Guo, W.; Peng, X. Experimental Determination of the Extinction Coefficient of CdTe, CdSe, and CdS Nanocrystals. *Chem. Mater.* **2003**, *15*, 2854–2860.
54. Aldana, J.; Wang, Y. A.; Peng, X. Photochemical Instability of CdSe Nanocrystals Coated by Hydrophilic Thiols. *J. Am. Chem. Soc.* **2001**, *123*, 8844–8850.
55. Schlenoff, J. B.; Ly, H.; Li, M. Charge and Mass Balance in Polyelectrolyte Multilayers. *J. Am. Chem. Soc.* **1998**, *120*, 7626–7634.
56. Tice, D. B.; Frederick, M. T.; Chang, R. P. H; Weiss, E. A. Electron Migration Limits the Rate of Photobrightening in Thin Films of CdSe Quantum Dots in a Dry N_2(g) Atmosphere. *J. Phys. Chem. C* **2011**, *115*, 3654–3662.